Crystallization and structure of high boron content iron–boron ultrafine amorphous alloy particles

Z. HU, Y. FAN, Y. WU, Q. YAN, Y. CHEN
Co-ordination Chemistry Institute and Department of Chemistry, Nanjing University, Nanjing 210093, People's Republic of China

Amorphous to crystalline transformation of chemically prepared $Fe_{64}B_{36}$ ultrafine amorphous alloy particles has been investigated by Mössbauer spectroscopy, Brunauer–Emmett–Teller surface area measurements and transmission electron microscopy. Structural relaxation was observed below 350 °C, which resulted in narrowing the full width at half maximum for the hyperfine field distribution from 13.0 to 10.6 T, while the average hyperfine field kept unchanged, to be about 20.3 T. Crystallization started on the surface at about 300 °C and proceeded into the bulk at about 400 °C. Partial crystallization between 400 and 450 °C resulted in increasing the average hyperfine field for the remaining Fe–B amorphous matrix to 21.6 T. α-Fe and Fe_2B were the only iron containing phases related to bulk crystallization, with the latter as a predominant component, accompanied by the segregation of about 19% boron atoms. Above 500 °C, sintering of the particles became very remarkable and a solid state reaction between diffusing iron and boron atoms to form Fe_2B took place making the spectral area ratio for Fe_2B to α-Fe components increase accordingly. A locally distorted non-stoichiometric Fe_2B quausicrystalline structure for the high boron content sample was proposed.

1. Introduction

Amorphous alloys, usually prepared in ribbon and film forms, have many unique properties, such as easy magnetization, superior corrosion resistance, high mechanical toughness and interesting electronic properties which stem from the long range disordered and short range ordered structure [1]. In the fields of metallurgy and magnetism, amorphous materials have already been practically utilized and they are increasingly produced for research and technological purposes [1]. In other fields, they have also shown great potential applications. For example, in catalysis, amorphous alloys have exhibited better selectivity and higher specific activity than their crystalline counterparts. However, the very small specific surface areas, σ, (usually $< 0.1 \, m^2 \, g^{-1}$) limits the development of their industrial use in this field [2]. The combination of ultrafine size with amorphous structure will probably solve this difficulty by greatly increasing σ ($\sim 20 \, m^2 \, g^{-1}$ [3]). In addition, ultrafine amorphous alloy particles have an inherent advantage over melt-spun ribbons or films, in that they are suitable for use in compaction processes, ferrofluids, magnetic memory systems and so on. These are important factors for increasing interest in ultrafine amorphous powders prepared by chemical methods [4–13]. No matter what field the new amorphous powders will be used in, thermal stability is a common topic of interest since many useful properties will disappear during

crystallization. It is also well known that as a first approximation the structure of transition metal–metalloid amorphous alloys can be described by dense random packing of hard spheres (DRPHS). The simplicity of this model often results in discrepancies between theoretical and experimental results in many aspects, as partially summarized by Kemeny *et al.* [14]. For Fe–B amorphous alloys, the locally distorted non-stoichiometric Fe_3B quausicrystalline structure was then proposed instead of DRPHS construction [14, 15]. However, it should be noted that most of the studied binary a-$Fe_{100-x}B_x$ samples were produced by the liquid quench technique and were in a narrow concentration range of $14 \leqslant x \leqslant 28$ [14–18]. Although amorphous $Fe_{100-x}B_x$ alloys have been previously fabricated by r.f. sputtering in a more wider composition range ($10 \leqslant x < 100$) [19, 20], gas contamination and internal stress in the sputtered film influence the intrinsic properties of them. Hitherto, little attention has been paid to the structure of a-$Fe_{100-x}B_x$, with $x \geqslant 33$, probably due to the difficulty in obtaining "free" or unsupported samples in the past [21]. By using the recently developed chemical method, a-$Fe_{100-x}B_x$, with $x \geqslant 33$, can be prepared conveniently [9], hence offering an opportunity to discuss its short range order. On the basis of the above, this paper studies the surface and bulk crystallization behaviour of $Fe_{64}B_{36}$ ultrafine amorphous powder mainly by Mössbauer spectroscopy,

Brunauer–Emmett–Teller surface area measurements (BET) and transmission electron microscopy (TEM). An Fe_2B-like short range order structure for the high boron content sample was proposed accordingly.

2. Experimental procedure

The ultrafine amorphous powder was prepared by dropwise addition of 100 ml 0.1 mol l^{-1} $FeSO_4 \cdot H_2O$ aqueous solution to 100 ml 0.4 mol l^{-1} KBH_4 solution within about 10 min under ultrasonic agitation at about 10 °C. The black precipitate was washed with distilled water, ethanol and acetone sequentially, then passivated in a nitrogen atmosphere with a trace of oxygen for $\sim$24 h. The composition of the powder was $Fe_{64}B_{36}$ as analysed by an inductively coupled plasma (ICP) method. The amorphous structure of the sample was confirmed by X-ray diffraction and selected area electron diffraction techniques. The as-prepared sample was thermally treated at several fixed temperatures from 100 to 700 °C for 2 h under high purity flowing argon. Mössbauer spectra were obtained at room temperature using a constant acceleration spectrometer with a 15 mCi source of $^{57}Co/Pd$. The spectra of the amorphous and partially amorphous samples were fitted using the method developed by Le Caër and Dubois [22] and a Lorentzian type peak shape was adopted. Since the samples were in ultrafine powder form, the magnetic moments were randomly orientated with weak coupling among them and no preferred orientation existed [10]. The intensity ratio of lines 2–5 to lines 1–6, I_{2-5}/I_{1-6}, was then constrained to 2/3, the theoretical value. The spectra of crystalline samples were fitted with the Mösfun program [23]. The isomer shifts are given relative to α-Fe at room temperature. The surface areas of the samples were measured by the BET method using nitrogen physisorption at 77 K with a Micromeritics ASAP 2000. The particle sizes and aggregate patterns of the samples were observed by TEM.

3. Results and discussion

Fig. 1 shows the Mössbauer spectra for the as-prepared and heat treated samples, together with the corresponding hyperfine field distributions, $P(H)$. The spectrum of the as-prepared sample exhibits a widely broadened sextet with lines 1 and 2 and lines 5 and 6 highly overlapping, and a broad $P(H)$ reflecting the amorphous structure and the high boron content of the sample. A central paramagnetic doublet ($\approx 5\%$ relative intensity, see Table I) with isomer shift (IS) of 0.35 mm s^{-1} and quadrupole splitting (QS) of 0.95 mm s^{-1} due to surface oxidation also exists [9, 10]. When the annealing temperatures, T_A, are lower than 350 °C, the Mössbauer spectra do not change obviously and the average hyperfine field ⟨H⟩ remains at about 20.3 ± 0.2 T; however, the full width at half maximum (FWHM) of the $P(H)$ decreases from about 13.0 T for the sample with $T_A \leqslant 300$ °C to 10.6 T for the sample with $T_A = 350$°C, due to structural relaxation of the amorphous phase [12]. Annealing at higher temperatures of 400 and 450 °C leads

to partial crystallization into α-Fe and Fe_2B with ⟨H⟩ for the remaining amorphous matrix increasing to 21.6 ± 0.2 T, thereby indicating a decrease of the boron content in the amorphous matrix [9], probably due to the segregation of boron atoms. The $P(H)$ curves for these two samples are somewhat anomalous in comparison with other $P(H)$ curves due to the difficulty of striping fully the crystalline components in fitting the Mössbauer spectra. Anyhow, there is a clear right shift of the hyperfine field distributions. The amorphous powder completely crystallizes at
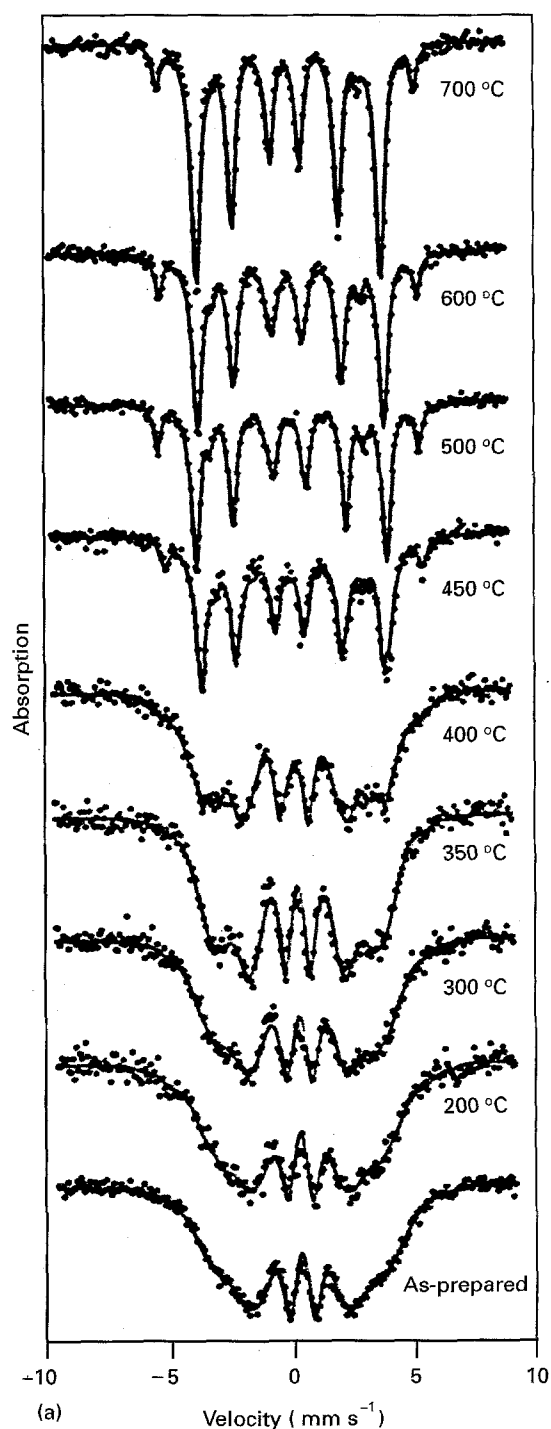

Figure 1 Mössbauer spectra (a) and corresponding hyperfine field distributions, $P(H)$, for amorphous components (b) of the samples as-prepared and after annealing in flowing Ar for 2 h at the indicated temperatures. The solid curves in (a) are the fitting results with the corresponding $P(H)$ in (b).
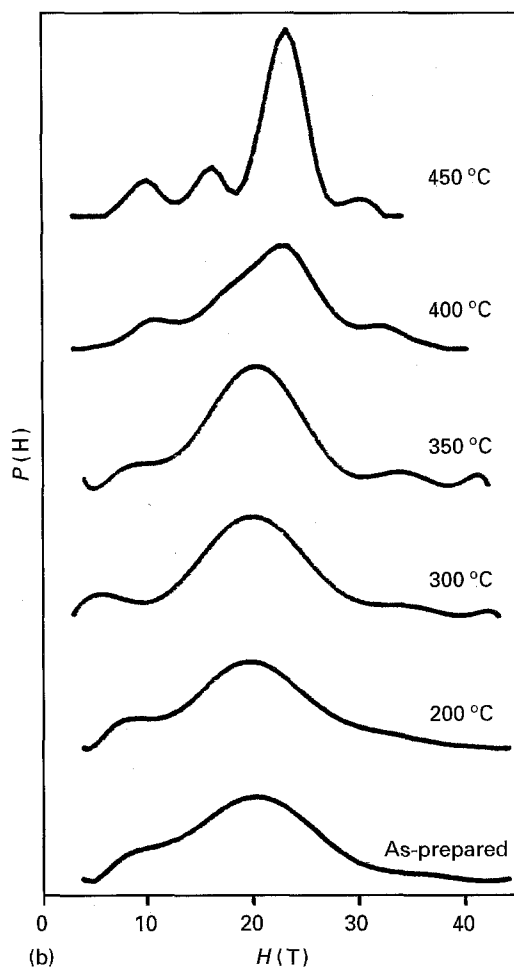
612

Figure 1 (*Continued*)

B atoms which separate during the initial stages of crystallization subsequently form Fe_2B by a solid state reaction [13]. This assumption is supported by the gradual increase of FWHM of lines 1 and 6 for α-Fe from 0.33 to 0.39 mm s^{-1} as indicated in Table I, which reflects that the increasing boron atoms in α-Fe lattice are an impurity. The solid state reaction is justifiable since a similar reaction has been observed at T_A as low as 350 °C in vacuum conditions [25]. In contrast, for the low boron content sample $Fe_{74}B_{26}$ [12], the relative peak intensity of Fe_2B with respect to α-Fe decreases with annealing temperature upon crystallization, and the segregated Fe and B atoms are much greater than those of the high boron content samples. Therefore, it is reasonable to argue that the tendency for changing the relative peak intensity of Fe_2B with respect to α-Fe is determined by competition between atomic segregation and the solid state reaction; and that the probability of the solid state reaction depends not only on the concentrations of the diffusing Fe and B atoms, but also on short range ordering of the amorphous matrix. The Fe_3B-like structure of the low boron content sample [14, 15] will change significantly, e.g. due to breaking and forming of the Fe–B bond, to give Fe_2B structure on annealing. During this step some Fe and B atoms segregate or recombine to form Fe_2B by diffusion. It is noticed that, unlike eutectic (α-Fe + Fe_3B) crystallization [14], the metastable Fe_3B phase does not appear at all during crystallization for the high boron content sample, in contradiction with the locally distorted non-stoichiometric Fe_3B quausicrystalline structure. The atomic ratio in the sample $Fe_{64}B_{36}$ is very close to that in Fe_2B. From Table I, it is seen that Fe_2B is a predominant crystallization product, implying that the formation of Fe_2B crystallites requires only a small reordering of the mother amorphous matrix. In other words, the Fe_2B-like structure would be the natural building element of the amorphous structure. In fact, previous experimental results [10] indicate that the chemical method itself favours the prenucleation formation of a Fe_2B phase. In such an Fe_2B structured matrix, the formation of Fe_2B species from reaction of diffusing Fe and B atoms should be much easier than in the case for the low boron content sample due to the "epitaxy" effect. Based on the above consideration, the apparent contradiction between the

$T_A \geqslant 500$ °C, with the relative peak intensity of Fe_2B with respect to α-Fe increasing with T_A (500–700 °C, Table I). The boron content in the iron containing phases has been estimated according to the spectral area ratio of the two components by ignoring the difference of the recoilless fraction between Fe and Fe_2B (Table I). The calculated boron content is less than that obtained by ICP. Apparently, the segregation of B atoms takes place, as observed previously, for heat treated amorphous Fe–B powders and ribbons [12, 13, 24]. The amount of Fe_2B increases with annealing temperature due to the fact that the Fe and

TABLE I The amount of α-Fe and Fe_2B deduced from Mössbauer spectroscopy as a function of annealing temperature. From these data the boron content in iron containing phases has been calculated.

T_A (°C)	A^a (%)	H^b (T)	α-Fe (%)	Fe_2B (%)	B^c (at %)	By	FWHM^d (mm s^{-1})
As-prepared	95	20.3	–	–	36	ICP	–
400	93	21.8	1	2	–	–	–
450	67	21.4	7	23	–	–	–
500	0	–	18	82	29	Mössbauer	0.33
600	0	–	16	84	30	Mössbauer	0.34
700	0	–	10	90	31	Mössbauer	0.39

[a] A, area percentage for Fe–B amorphous matrix in Mössbauer spectra.
[b] H, average hyperfine magnetic field of Fe–B amorphous matrix.
[c] About 19% B atoms [(36–29)/36] segregated from amorphous matrix due to crystallization at 500 °C.
[d] FWHM, full width at half maximum of lines 1 and 6 for α-Fe component.

effect of annealing on high and low boron content samples may be understood.

From the Mössbauer experimental results, it seems that the amorphous $Fe_{64}B_{36}$ sample begins to crystallize at about 400 °C. However, it should be kept in mind that transmission Mössbauer spectroscopy is only sensitive to bulk structure. Structural change on the surface of the particles has to be probed by other means.

Curve a in Fig. 2 shows the BET specific surface area, σ, versus annealing temperature, T_A. It is seen that four stages can be distinguished. The value of σ increases with T_A up to 200 °C (stage I), this is followed by a decrease up to 300 °C (stage II), then a relatively steady period appears up to 400 °C (stage III) and, finally, σ sharply decreases again when $T_A \geqslant 400$ °C (stage IV). The four stage phenomenon was confirmed, as seen from curve b in Fig. 2, by *in situ* measurement of σ in a BET apparatus under vacuum conditions (pressure 53 $N m^{-2}$), where a fixed amount of the as-prepared sample was heated at several temperatures from low to high sequentially for 2 h, with σ obtained after each treatment. Although the temperature range for each stage in curve b is a little lower than the corresponding one in curve a, due to the difference in annealing environment and procedure, the trends of both curves are fairly similar. The information on surface change contained in each stage may be deduced by referring to the changing behaviour of the bulk phase as monitored by Mössbauer spectroscopy and to the aggregate patterns of the particles seen in the TEM photographs of Fig. 3.

The aggregate pattern of the as-prepared sample (Fig. 3a) indicates an unseparated "cotton-like" picture, as reported by other authors [10], which may arise from a connection effect of the impurity absorbed on the particle surface during preparation and passivation, resulting in partial covering of particle surfaces. The connection "network" collapses during
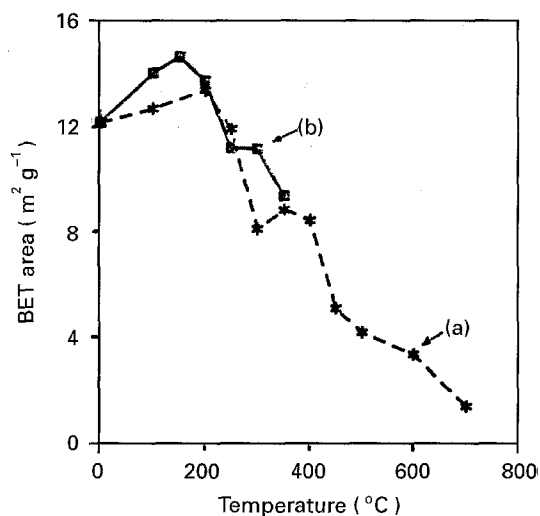

Figure 2 The profile of the specific surface areas of the $Fe_{64}B_{36}$ samples versus annealing temperature. Curve (a) each sample for σ measurement was obtained by annealing the as-prepared powder under flowing Ar gas for 2 h, curve (b) each σ was measured with a fixed amount of powder after *in situ* annealing sequentially in vacuum condition.

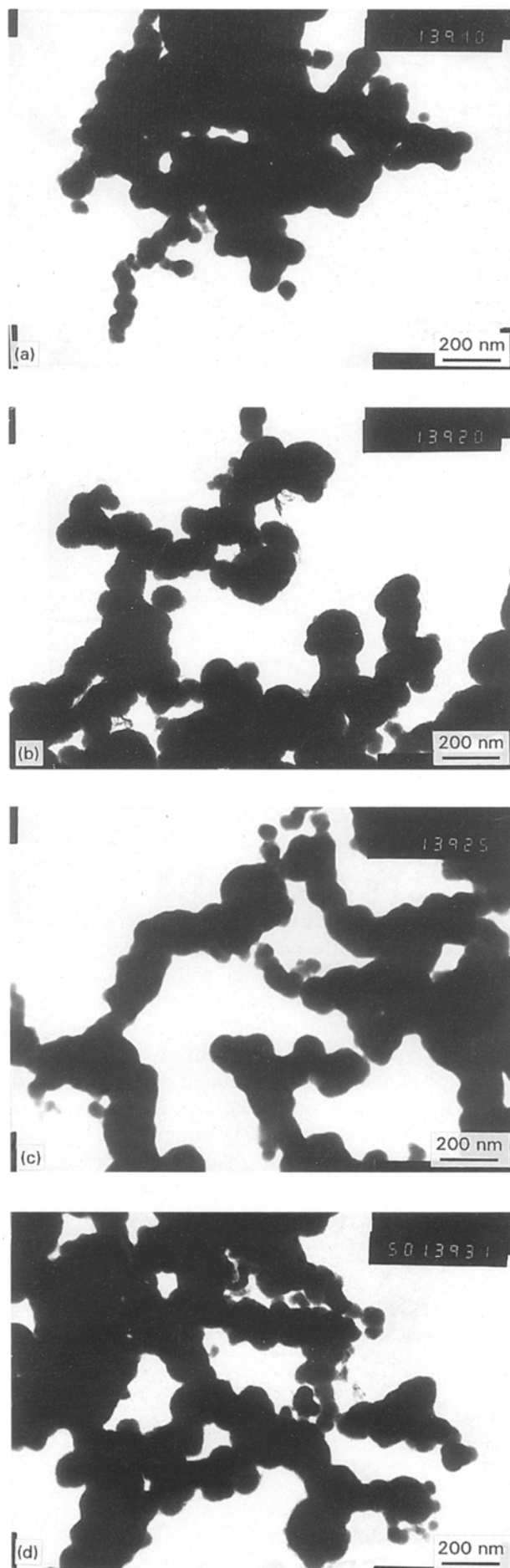*Figure 3* Typical transmission electron microscopic photographs of the $Fe_{64}B_{36}$ samples as-prepared (a) and after annealing at different temperatures as follows: (b) 200 °C, (c) 300 °C, (d) 400 °C, (e) 450 °C, (f) 500 °C, and (g) 700 °C.
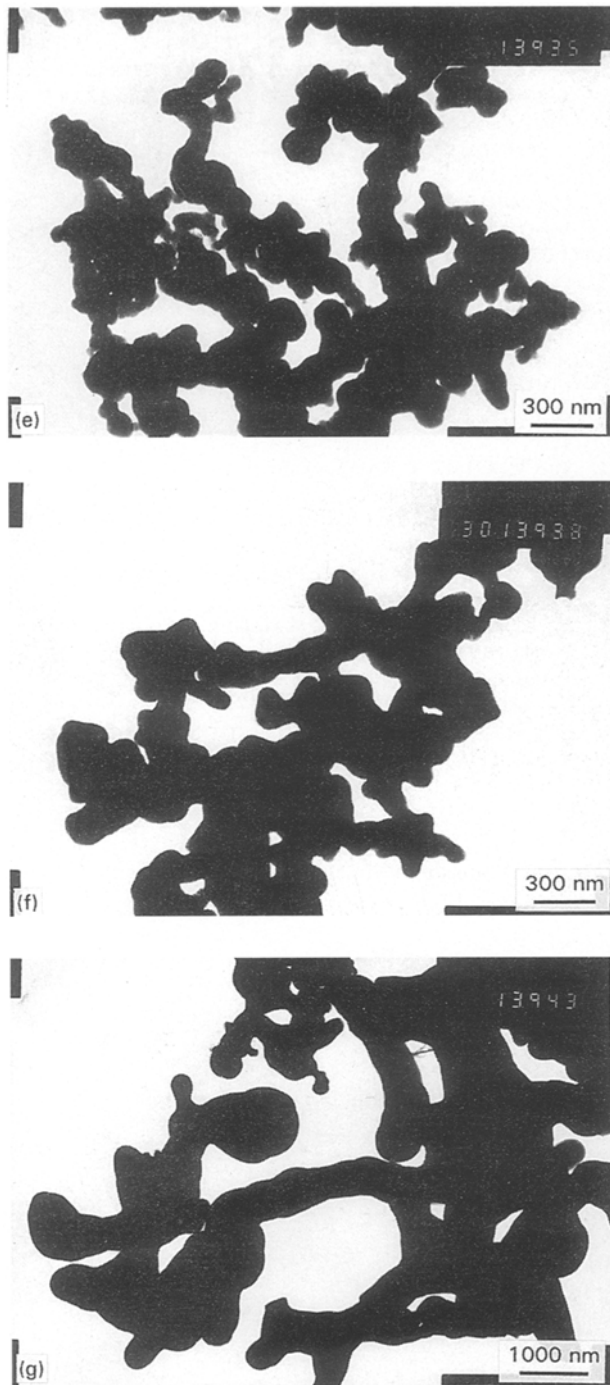
(e) 300 nm

(f) 300 nm

(g) 1000 nm

Figure 3 (Continued)

thermal treatment at stage I, the aggregate pattern turns from "cotton-like" into "chain-like" (Fig. 3b) and some covered particle surfaces are released. As a result, σ increases with T_A at stage I. At this stage, the particle size is observed to be less than 150 nm. At

stage II, slight sintering of the particles takes place which results in decreasing σ with T_A. At stage III, crystallization on the particle surface is believed to start, and many microcrystals embedded in the remaining amorphous matrix increase the roughness of the particle surface and thereby σ, in a similar way to the case of $Cu_{70}Zr_{30}$ amorphous ribbon [26]. In fact, crystallization starting from the surface and proceeding into the interior of an Fe–B ribbon was also observed and directly determined by conversion electron Mössbauer experiments [24]. The surface roughness and particle sintering have opposite effects on σ, and competition between the two factors makes σ changes with T_A more steadily at stage III than at the other three stages. In the early period of stage IV (400–500 °C), it is observed, from Mössbauer results, that bulk crystallization begins to take place. Thus it is reasonable to consider that the surface microcrystals, which can be formed at lower temperatures (stage III), would grow at this time. Meanwhile, the sintering factor becomes more significant. These two factors result in a sharp decrease of σ. Bulk crystallization is accompanied by the segregation of about 19% boron atoms. The sintering effect becomes more and more remarkable at higher T_A as obviously observed from the morphological change of the particles (Fig. 3d–g), which increases atomic mobility and results in increasing recombination of the diffusing Fe with B atoms to form Fe_2B.

4. Conclusions

High boron content $Fe_{64}B_{36}$ amorphous powder with particle sizes less than 150 nm has been prepared by the chemical reduction method. Structural relaxation in the low temperature range ($\leqslant 350$ °C) caused the narrowing FWHM of hyperfine field distribution. The crystallization process begins at the particle surface and proceeds into the bulk. Since the atomic ratio of boron to iron approaches $1:2$ as in Fe_2B, the crystallization products are different from those for amorphous Fe–B with lower boron content reported in the literature. Combining the experimental results obtained by Mössbauer spectroscopy, BET and TEM, the crystallization configuration for $Fe_{64}B_{36}$ amorphous powder could be approximately elucidated as shown in Table II.

The majority of the crystallization products are Fe_2B, and the metastable Fe_3B phase does not appear during crystallization. An Fe_2B-like structure of short range order for a-$Fe_{64}B_{36}$ is, therefore, proposed.

TABLE II Crystallization configuration for $Fe_{64}B_{36}$

Stage	Temperature range (°C)	Physical processes	Phenomena
I	0–200	Collapse of connection "net"	Increase of σ
II	200–300	Slight sintering and structural relaxation	Decrease of σ
III	300–400	Structural relaxation, crystallization on surface, sintering	Surface roughness, steady σ
IV(1)	400–500	Growth of surface microcrystals, bulk crystallization	Sharp decrease of σ, α-Fe + Fe_2B + B
IV(2)	500–700	Solid state reaction between defusing Fe and B atoms, remarkable sintering	Further decrease of σ

615

References

1. F. E. LUBORSKY "Amorphous Metallic Alloys" (Butterworth, London, 1983).
2. A. MOLNAR, G. V. SMITH and M. BARTOK, *Adv. Catal.* **36** (1989) 329.
3. Y. FAN, Z. HU, J. SHEN, Q. YAN and Y. CHEN, *J. Mater. Sci. Lett.* **12** (1993) 596.
4. J. VAN WONTERGHEM, S. MORUP, C. J. W. KOCH, S. W. CHARLES and S. WELLS, *Nature* **322** (1986) 622.
5. J. VAN WONTERGHEM, S. MORUP, S. W. CHARLES, S. WELLS and J. VILLADSON, *Phys. Rev. Lett.* **55** (1985) 410.
6. Z. HU, Y. FAN, Y. WU, Q. YAN and Y. CHEN, *J. Magn. Magn. Mater.* **140–144** (1995) 413.
7. Z. HU, J. SHEN, Y. CHEN, M. LU and Y. HSIA, *J. Non-Cryst. Solids* **159** (1993) 88.
8. Z. HU, Y. CHEN and Y. HSIA, *Nucl. Instrum. Meth. Phys. Res. B* **76** (1993) 121.
9. Z. HU, Y. FAN and Y. CHEN, *Mater. Sci. Eng. B* **25** (1994) 193.
10. J. JIANG, I. DEZSI, U. GONSER and J. WEISSMULLER, *J. Non-Cryst. Solids* **116** (1990) 247.
11. S. LINDEROTH and S. MORUP, *J. Appl. Phys.* **69** (1991) 5256.
12. S. LINDEROTH, *J. Magn. Magn. Mater.* **104–107** (1992) 128.
13. S. LINDEROTH, S. MORUP, A. MEAGHER, J. LARSEN, M. D. BENTZON, B. S. CLAUSEN, C. J. W. KOCH, S. WELLS and S. W. CHARLES, *ibid.* **81** (1989) 138.
14. T. KEMENY, I. VINCZE, B. FOGARASSY and S. ARAJS, *Phys. Rev. B* **20** (1979) 476.
15. I. VINCZE, D. S. BOUDREAUX and M. TEGZE, *ibid.* **19** (1979) 4896.
16. C. L. CHIEN, D. MUSSER, E. M. GYORGY, R. C. SHERWOOD, H. S. CHEN, F. E. LUBORSKY and J. L. WALTER, *ibid.* **20** (1979) 283.
17. C. L. CHIEN, *ibid.* **18** (1978) 1003.
18. R. OSHIMA and F. E. FUJITA, *Jpn. J. Appl. Phys.* **20** (1981) 1.
19. H. HOVING, F. VAN DER WOUDE, K. BUSCHOW and I. VINCE, *J. Non-Cryst. Solids* **61/62** (1984) 421.
20. C. L. CHIEN and K. M. UNRUH, *Phys. Rev. B* **24** (1981) 1556.
21. T. NAKAJIMA, I. NAGAMI and H. INO, *J. Mater. Sci. Lett.* **5** (1986) 60.
22. G. LE CAËR and J. M. DUBOIS, *J. Phys. E, Sci. Instrum.* **12** (1979) 1083.
23. E. W. MULLER, *Mössbauer Effect Reference Data J.* **4** (1981) 89.
24. M. ACKERMANN, H.-G. WAGNER, U. GONSER and P. STEINER, *Hyperfine Interactions* **27** (1986) 397.
25. J. JING, S. J. CAMPBELL, A. CALKA and A. V. J. EDGE, *ibid.* **69** (1991) 475.
26. A. BAIKER, H. BARIS and H. J. GUNTHERODT, *Appl. Catal.* **22** (1986) 389.